# CHAPTER 15

# Quantitative and Qualitative Analysis of Plant Membrane Traffic Using Fluorescent Proteins

**Marketa Samalova, Mark Fricker, and Ian Moore**

Department of Plant Sciences
University of Oxford
Oxford OX1 3RB
United Kingdom





METHODS IN CELL BIOLOGY, VOL. 85


0091-679X/08 $35.00
DOI: 10.1016/S0091-679X(08)85015-7

## Abstract

Fluorescent proteins have had a great impact on the way in which plant membrane traffic is studied. Here we review the uses to which these molecules have been put in this field of research and discuss the advantages and pitfalls of particular fluorescent protein derivatives in various applications and plant species. We discuss in detail the need for quantitative estimates of expression level and the potential of fluorescent proteins for quantitative assays of biosynthetic membrane traffic. Detailed descriptions and protocols are provided for the use of the newly developed 2A-based ratiometric polyprotein probes of membrane traffic in conjunction with semiautomated image analysis software packages for quantitative analyses. The ratiometric probes and software are available from the authors.

## I. Introduction

In recent years, studies of membrane traffic and endomembrane organization in plant cells have made increasing use of intrinsically fluorescent proteins (IFPs) to visualize several endomembrane organelles (Brandizzi *et al*., 2002, 2004; Zheng *et al*., 2005) and to isolate mutants with altered endoplasmic reticulum (ER) morphology (Matsushima *et al*., 2003; Tamura *et al*., 2005). Green fluorescent protein (GFP) has also been used as a marker of biosynthetic traffic to the apoplast or the vacuole in plants (Batoko *et al*., 2000; Boevink *et al*., 1998; DaSilva *et al*., 2004, 2005; Flückiger *et al*., 2003; Geelen *et al*., 2002; Kotzer *et al.,* 2004; Lee *et al*., 2004; Sohn *et al*., 2003; Takeuchi *et al*., 2000; Zheng *et al*., 2004, 2005). As GFP fails to accumulate in a fluorescent form in either destination (Batoko *et al*., 2000; Boevink *et al*., 1999; Tamura *et al*., 2003), perturbation of anterograde traffic is readily visualized by the accumulation of fluorescence in upstream compartments such as ER, the Golgi apparatus, or prevacuolar compartments (PVC). This strategy is effective in transformed mutant *Arabidopsis* seedlings (Tamura *et al*., 2005; Zheng *et al*., 2004) but has been used most frequently in transient expression studies to investigate the effect of genetically dominant derivatives of putative membrane trafficking proteins or of inhibitors. Thus in principle xFP-based assays can provide qualitative morphological information on the steps of the pathway that are disrupted and quantitative information on the extent to which trafficking is disrupted. Genuinely quantitative studies are rare however.

The utility of fluorescent proteins in each of these applications is critically dependent on several of their photochemical and biological properties. Table I summarizes important properties of several fluorescent proteins that are commonly used for membrane trafficking research. Commercially available proteins now span almost the entire visible range and some noncommercial alternatives or derivatives offer significant advantages. These are discussed further below.

## A. Photochemical and Biological Properties of IFPs

The native GFP coding sequence was prone to misexpression in *Arabidopsis* owing principally to the presence of a cryptic intron. This was eliminated by the site-directed mutagenesis in a series of GFP derivatives (mGFP4-mGFP6) generated by Jim Haseloff and colleagues (http://www.plantsci.cam.ac.uk/Haseloff/imaging/GFP.htm). However, the codon modifications introduced into the commercial IFPs for optimization of expression in animal cells also eliminate missplicing, and these can be expressed efficiently in *Arabidopsis* and other plant cells. The commercial IFPs, with the exception of DsRed, can also be used effectively in the plant endomembrane system. DsRed exists as a tetramer, and this property often causes fusion proteins to aggregate in a concentration-dependent manner. This can cause significant disruption to endomembrane organelles. Although DsRed can be used with caution (Saint-Jore *et al.*, 2002), the monomeric derivative mRFP1 (Campbell *et al.*, 2002) is preferable by far and has been used in several studies to mark endomembrane organelles (Lee *et al.*, 2002; Samalova *et al.*, 2006; Zheng *et al.*, 2005).

In common with other applications of IFPs, an important consideration is the relative brightness of each protein. Yellow fluorescent protein (YFP) is 50% brighter than GFP and at least three times brighter than cyan fluorescent protein (CFP) or mRFP1. This is important in localization studies as the intrinsic brightness of a protein establishes a minimal abundance for detection with any given imaging system, and this may or may not be similar to the native abundance of the tagged molecule. Thus it will be possible to image a fluorescent fusion to YFP at threefold lower expression levels than the equivalent red fluorescent protein (RFP) or CFP fusion, with correspondingly reduced risks of overexpression artifact. Another advantage to the use of YFP is the existence of diverse GFP-based fusions that can be used for colocalization studies with imaging systems that allow these two fluors to be discriminated effectively. Indeed, one of the major applications of IFPs is in colocalization studies involving multifluorescent imaging of two or more proteins.

Satisfactory discrimination of IFPs using conventional mirrors and filters is usually dependent on selective excitation as well as selective detection. Two non-commercial IFP derivatives offer significant advantages in this regard. The first of these is mGFP5 (Table I) that exhibits an increase in the 480 nm excitation peak but without either the redshift or loss of the 400 nm peak that characterize EGFP. This provides more efficient excitation with the 458 and 405 nm lasers on confocal systems, allowing for increased discrimination from YFP or mRFP1. For these reasons, we routinely use mGFP5 for all our GFP work. The second protein with useful spectral properties is mRFP1, which is redshifted for emission and excitation relative to DsRed (Table I). This provides for more efficient discrimination from YFP and GFP which each have long emission tails and excitation spectra that overlap the short-wavelength shoulder of the DsRed and mRFP1 spectra. A derivative, mCherry, offers similar spectral characteristics but with improved brightness and photostability and is now likely to be the protein of choice (Table I).

For most combinations of IFP, sequential excitation is required to discriminate the two fluors. When imaging organelles in live plant cells, this requires the use of a

**Table I**
**Photochemical and Biological Properties of Fluorescent Proteins**

| FPs | $Ex_{max}$ (nm) | $Em_{max}$ (nm) | Relative brightness | $pK_a$ | Note Ex laser (nm) | Note | Ref. |
|---|---|---|---|---|---|---|---|
| ECFP (CFP) | 430 | 475 | 3 | <5.0 | 405,458 | – | Clontech |
| mGFP5 | 405/477 | 508 | ? | <5.0 | 405,458,488,(477) | Maybe dimmer than EGFP | [a] |
| EGFP | 488 | 508 | 8 | 5.5 | 458,488,(477) | – | Clontech [d] |
| EYFP (YFP) | 514 | 527 | 12 | 7.0 | 488,514 | $Cl^-$ sensitive | Clontech [d] |
| Venus YFP | 515 | 528 | 13 | 6.1 | 488,514 | Less $Cl^-$ sensitive but also less photostable | [b,d] |
| DsRed | 550 | 580 | 15 | <5.0 | – | aggregates | Clontech |
| mRFP1 | 580 | 610 | 3 | <5.0 | 514,543(488) | Protease insensitive | [c]. |
| mCherry | 587 | 610 | 4 | <4.5 | 543 | – | [d]. |
| mPlum | 590 | 649 | 1 | <4.5 | – | – | [d]. |

[a]Haseloff, J. <http://www.plantsci.cam.ac.uk/Haseloff/imaging/GFP.htm>
[b]Nagai *et al.* (2002).
[c]Campbell *et al.* (2002).
[d]Shaner *et al.* (2005).

confocal laser scanning microscope with line-sequential scanning capability. This is because streaming in the cytoplasm of vacuolate plant cells is too fast (ca. 5 $\mu$m/s) for frame sequential imaging, even with electronic switching between detection channels. In the absence of a line-sequential scanning system, unless cells are fixed, only a limited range of IFP combinations can be used for simultaneous detection. These include CFP with either YFP or mRFP1, and mGFP5 with mRFP1. However, in our experience the long emission tail of mGFP5 results in significant bleed-through when its abundance is high relative to that of mRFP1, and we usually use a line-sequential scanning routine with 458 nm (mGFP5) and 543 nm (mRFP1) excitation lines when imaging with this pair. The redshifted, normalized excitation spectrum of EGFP relative to mRFP1 predicts that bleed-through may be greater with this fluor (Fig. 1).

With sequential excitation at 458 and 514 nm, it is possible to discriminate mGFP5 and YFP satisfactorily in most applications (Samalova *et al.*, 2006). The configuration we routinely use for this on a Zeiss LSM510 confocal is outlined in Fig. 2. When mGFP5 signals are weak relative to YFP, bleed-through into the GFP channel can nevertheless be an issue as YFP is excited to about 3% of maximum by the 458 nm line and a correction may be required. Alternatively, if a 405 nm excitation line is available, this can in principle be used to selectively excite mGFP5, but we have found that some plant cells such as tobacco leaf epidermis exhibit significant autofluorescence in the GFP range when illuminated by 405 nm light. Sequential excitation with 458 and 514 nm lines can also be used to image EGFP and YFP within a narrow range of relative abundance at least

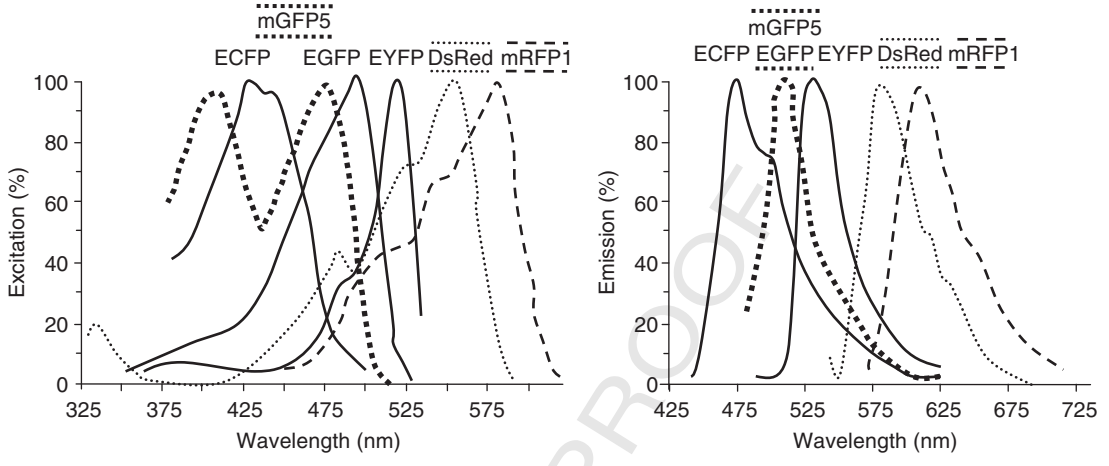


**Fig. 1** Excitation and emission spectra of fluorescent proteins. Normalized excitation and emission spectra for proteins discussed in the text. Data extracted from the sources listed in Table I.

(L. Camacho and I. Moore, University of Oxford, Oxford, UK, unpublished). With this combination of fluors, bleed-through from GFP to YFP is also a concern owing to the greater excitation of EGFP at 514 nm, so the EGFP signal in the specimen needs to be relatively weak. The ability to discriminate these fluors at all is perhaps surprising given the normalized spectra shown in Fig. 1. The relative brightness of EGFP and mGFP5 is unknown; however, so it is possible that the weaker excitation of EGFP than mGFP5 by 458 nm light is compensated by an increased brightness. Nevertheless, rigorous bleed-through controls are essential when using EGFP and YFP, so mGFP5 or ECFP are preferable partners for YFP.

An important consideration when working with IFPs in the endomembrane system is the pH sensitivity of their fluorescence. Table I shows that YFP has the highest $pK_{a,}$ which means it will exhibit minimal fluorescence even in weakly acidic compartments. Consequently, the location of a fusion protein that carries YFP on the luminal face of an endomembrane compartment may be misrepresented by YFP fluorescence. This has been illustrated well by the coexpression of equivalent secreted mGFP5 and YFP fusions in tobacco epidermal cells that revealed both proteins in the ER but only mGFP5 was detectable in post-Golgi compartments and cell wall (Zheng *et al.*, 2005). A variant of YFP, Venus, has a 10-fold lower $pK_a$ and is also effectively chloride insensitive (Table I), so it is preferable to EYFP when these parameters are critical but note that it is far less photostable than EYFP. Also note that the plant cell wall, vacuole, and PVC can have the pH values well below 6 (Grignon and Sentenac, 1991), so YFP can be used with confidence only in the ER and the Golgi (Zheng *et al.*, 2005) or on the cytoplasmic face of transmembrane proteins. Some membrane proteins carrying GFP derivatives on their cytoplasmic face have been observed to form large inclusions in both plant and animal cells however (Irons *et al.*, 2003; Runions *et al.*, 2006; Snapp *et al.*, 2003).

A

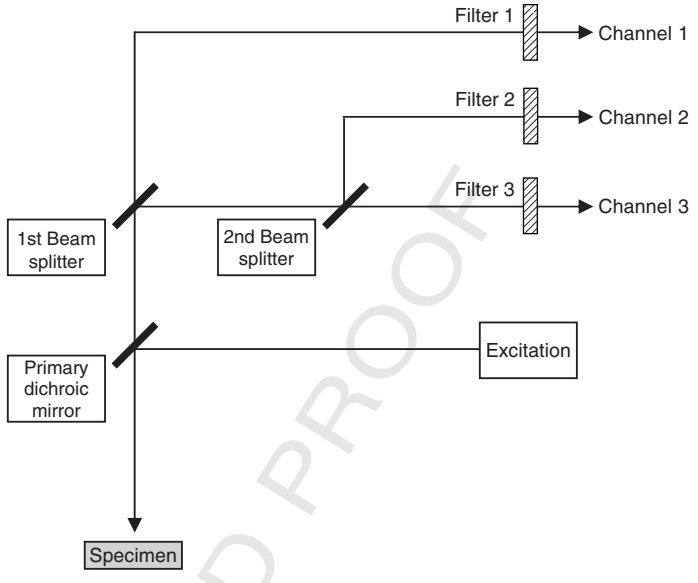


B

| FPs | Ex (nm) | Primary dichroic mirror | 1st Beam splitter | 2nd Beam splitter | Filters | Channels |
|---|---|---|---|---|---|---|
| **mGFP5**<br>**YFP**<br>chlorophyll | 458<br>514 | HFT 458/514 | NFT 635vis | NFT 515 | 1. LP 650<br>2. BP 475-525<br>3. BP 535-590IR | 1. chlorophyll (track 1)<br>2. mGFP5 (track 1)<br>3. YFP (track 2) |
| **mGFP5**<br>**mRFP1**<br>chlorophyll | 458<br>543 | HFT 458/543 | NFT 635Vis | NFT 545 | 1. LP 650<br>2. BP 475-525<br>3. BP 585-615 | 1. chlorophyll (track 1)<br>2. mGFP5 (track 1)<br>3. mRFP1 (track 2) |
| **mRFP1**<br>**YFP**<br>**mGFP5** | 543<br>514<br>405 | HFT 458/543 | NFT 635Vis | NFT 515 | 1. BP 592-635<br>2. BP 475-525<br>3. BP 535-590IR | 1. mRFP1 (track 1)<br>2. mGFP5 (track 3)<br>3. YFP (track 2) |
| **mRFP1**<br>**YFP**<br>**mGFP5** | 543<br>514<br>458 | NT 80/20 | NFT 545 | NFT 515 | 1. BP 581-635<br>2. BP 500/20IR<br>3. BP 535-590IR | 1. mRFP1 (track 1)<br>2. mGFP5 (track 3)<br>3. YFP (track 2) |

**Fig. 2** Suggested confocal configurations for dual and triple fluorescent labeling. (A) Simple schematic diagram of confocal optical configuration showing the elements referred to in B. (B) Table listing the multitrack (sequential imaging) configurations used for imaging pairs of fluorescent proteins. Individual laser lines and detection channels are switched on and off in sequence as each y-line in the image is scanned in each track, configurations are taken from Samalova *et al.* (2006).

The pH sensitivity of YFP has been exploited to probe the topology of a plasma membrane protein as fluorescence is observed only when the fluor is present in an internal loop (Swarup *et al*., 2004). Immmunodetection can be used to confirm the PM localization of nonfluorescent proteins. A similar strategy may be applied to membrane proteins of other acidic organelles. As discussed below, the pH sensitivity of IFPs can also be exploited to develop visual and quantitative assays of biosynthetic membrane traffic. EGFP is less pH sensitive than EYFP (Table I), but CFP, mGFP5, and particularly mRFP1 are the proteins of choice in this respect.

In addition to the intrinsic pH sensitivity of the fluorophore, GFP derivatives suffer pH- and light-dependent proteolysis in the plant vacuole (Tamura *et al*., 2003). Similar observations have been made with respect to the cell wall in tobacco, *Arabidopsis*, and onion epidermis (Batoko *et al*., 2000; Kamiya *et al*., 2006; Scott *et al*., 1999; Zheng *et al*., 2005). In each case, incubating material in the dark or in higher pH media restored fluorescence and protein accumulation in the cell wall or vacuole. The membrane-permeant protease inhibitor E64-d can be used to stabilize GFP in the vacuole of *Arabidopsis* and tobacco leaves (Tamura *et al*., 2003; Zheng *et al*., 2005). In the cell wall, a relatively stable degradation product appears to lack $\sim$1 kDa from the C-terminus and the ratio of full-length-to-processed-GFP can therefore act as an indicator of trafficking efficiency to the cell wall (Zheng *et al*., 2004). In contrast to the sensitivity of GFP derivatives, mRFP1 is apparently resistant to both the pH and the proteolytic environment of the cell wall and vacuole. In our experience, derivatives of mRFP1 targeted to either location have readily been detected, accumulating to high level and remaining stable for several days after transient expression (Samalova *et al*., 2006; Zheng *et al*., 2005).

## B. Vacuolar Sorting Signals in IFPs

Fluorescent proteins are often fused to plant proteins or protein sorting signals with a view to determining their localization in the endomembrane system. In addition to the usual caveats about the effects of tagging on native sorting signals or on protein folding and ER export, an assumption implicit in these experiments is that the IFP has no active sorting determinants. In the case of plant secretory and vacuolar traffic, this assumption can be unsafe. Zheng *et al.* (2005) have shown that a proportion of a secreted mGFP5 molecule, secGFP, is sorted to the vacuole of tobacco leaf epidermal cells where it can be visualized if the leaves are incubated in the dark with the protease inhibitor E64-d. The secGFP molecule studied by Zheng *et al.* (2005) has a c-myc epitope tag at its C-terminus that could carry the vacuolar sorting signal. However, our unpublished analysis of various GFP and mRFP1 derivatives locates the sorting signal to the GFP moiety (J. Legen and I. Moore, University of Oxford, Oxford, UK, unpublished). Similarly in yeasts, GFP is sorted efficiently to the vacuole by a Vps10-mediated pathway (Kunze

*et al.*, 1999). As GFP stability and fluorescence are weak in both the cell wall and the vacuole, the partial targeting of secGFP molecules to the plant vacuole does not compromise its use as a reporter of biosynthetic traffic between the ER and the *trans*-Golgi. By contrast, its use to report inhibition of post-Golgi secretory events may well be compromised by the ability of the protein to escape to the vacuole where it is unstable. Indeed, Zheng *et al.* (2005) showed that a dominant-negative mutant in a Rab-E GTPase, which was proposed to act between the Golgi and the PM, caused a relatively small increase in the secGFP accumulation compared with mutants that inhibited the secretory pathway upstream of the Golgi. At the same time, there was an increase in the amount of secGFP trafficked to the vacuole, so the weaker accumulation of secGFP appears to be attributable in part to its continued traffic to the vacuole when the secretory route is impaired (Zheng *et al.*, 2005).

In contrast to the secGFP marker discussed above, a secreted mRFP1 derivative used in the same study was found exclusively in the cell wall of tobacco leaf epidermis (Zheng *et al.*, 2005) (Fig. 3G). mRFP1 is readily visualized in the vacuole of tobacco epidermal cells when provided with a vacuolar sorting signal (Samalova *et al.*, 2006) (Fig. 3H), so it appears clear that mRFP1 lacks the serendipitous sorting signal of mGFP5. The same observations have been made in transgenic *Arabidopsis* leaves and roots (Samalova *et al.*, 2006; O. Teh and I. Moore, University of Oxford, Oxford, UK, unpublished observations). This, together with the high stability of mRFP1 in both the cell wall and the vacuole, makes mRFP1 the fluorescent protein of choice to study targeting to the vacuole or cell wall or in reporters of vacuolar sorting. It does not however provide the same quantitative change in fluorescence that is associated with the secretion of GFP, so it is a less convenient marker for studies of secretion. The pH-sensitive derivatives of mRFP1 are available (Shaner *et al.*, 2005), and these may provide ideal constructs for the assay of biosynthetic traffic to the cell wall.

The situation is however more complex as the vacuolar sorting of IFPs may be dependent on the experimental system used. In transgenic *Arabidopsis* plants, Zheng *et al.* (2004) found no evidence for the vacuolar accumulation of the same secGFP marker that is accumulated in the vacuoles of tobacco leaf epidermal cells. A small proportion of an ER-resident mGFP5 derivative, GFP-HDEL, could however be detected in the vacuole, consistent with reports that escaped ER residents are usually delivered to the vacuole (Tamura *et al.*, 2004). The differing behavior of secGFP in these studies may reflect species differences or the different expression systems (stable transgenic plants vs transient expression). In both these species, secreted mRFP1 molecules were excluded from vacuoles; however, Yang and colleagues report that secreted mRFP1 is transported with high efficiency to the vacuoles of transgenic tobacco BY-2 suspension cultured cells (Yang *et al.*, 2005). The reason for this difference is unclear, but these findings highlight the need for caution when applying IFPs to study trafficking in any new system.

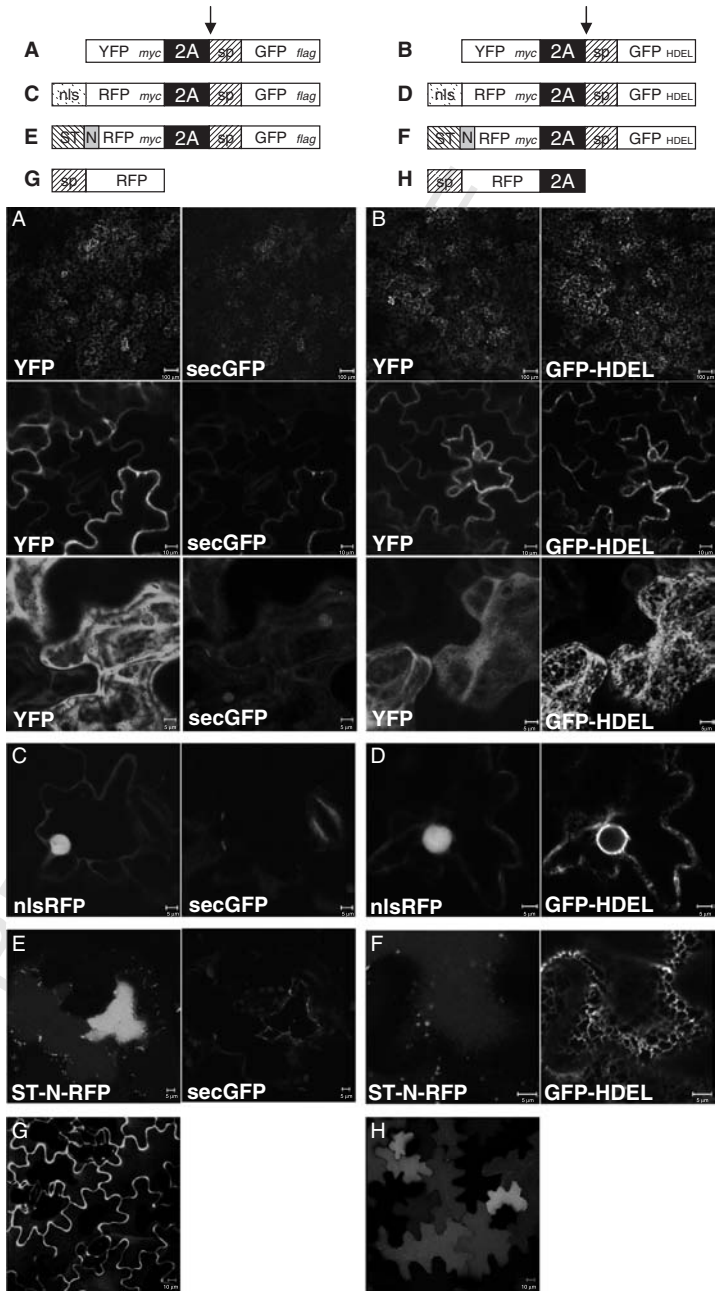


**Fig. 3** Selected examples of FMDV-2A-constructs for stoichiometric expression of two proteins. Schematic representation and confocal images of tobacco leaf epidermal cells transiently expressing (A) $Y_m$-2A-sec$G_f$, (B) $Y_m$-2A-GH, (C) nls$R_m$-2A-sec$G_f$, (D) nls$R_m$-2A-GH, (E) STN-$R_m$-2A-sec$G_f$,

## II. Rationale

### A. Need to Control Expression Level

In both quantitative and qualitative assays, it is important that the marker does not itself perturb the trafficking process. However, the expression level of a marker can influence the intracellular distribution of itself and other proteins. For example during the early stages of transient expression, secreted, vacuolar, and the Golgi-localized markers are present in the ER to varying degrees, depending on the expression efficiency in individual cells (Batoko *et al.*, 2000; Di Sansebastiano *et al.*, 1998; Flückiger *et al.*, 2003; Zheng *et al.*, 2005). Furthermore, the retrieval of proteins to the ER and sorting to the vacuole is dependent on the protein–protein interactions that can become saturated (DaSilva *et al.*, 2005; Frigerio *et al.*, 1998). In transient expression studies, these considerations demand that the transfection rates are kept low. Given the stochastic nature of the transfection process, this inevitably leads to a wide cell-to-cell variation in marker expression. Consequently, images of individual cells represent essentially anecdotal evidence and the effect of a transgene on trafficking can be inferred only from analyses of large cell populations. In the absence of a simple quantitative metric, performing and presenting such analyses are not straightforward. When transfection efficiencies are low or when high-magnification imaging is required to image changes in marker distribution or organelle morphology, analyses often rely on the subjective scoring of individual cells in the population (Kotzer *et al.*, 2004; Lee *et al.*, 2004; Sohn *et al.*, 2003; Zheng *et al.*, 2005). In such cases, the variability in the coexpression of marker and test constructs significantly complicates the analysis. Even when the test construct can be tagged with a visible marker, the expression level of the trafficked marker cannot be known. With higher-efficiency transfection procedures such as *Agrobacterium*-mediated expression in tobacco leaf epidermis and low-magnification images encompassing multiple-transfected cells may be sufficient to illustrate major changes in marker accumulation or distribution between treatments (Batoko

(F) STN-$R_m$-2A-GH, (G) secRFP, and (H) secRFP-2A. (A–H) The components of each construct are named and illustrated according to the following scheme: G or GFP = green fluorescent protein (mGFP5); Y or YFP = yellow fluorescent protein; R or RFP = red fluorescent protein (mRFP1); sp = signal peptide; sec = secreted form of fluorescent protein; H or HDEL = presence of endoplasmic reticulum (ER) retrieval signal in addition to signal peptide; nls = nuclear localization signal; ST = Golgi-targeting signal from rat sialyl transferase; N = engineered *N*-glycosylation site (Batoko *et al.*, 2000); $_m$ or myc = c-myc epitope tag; $_f$ or flag = FLAG epitope tag; 2A = foot and mouth disease virus (FMDV) 2A peptide, sequence taken from the constructs described by Halpin *et al.* (1999); the arrow indicates the site at which 2A activity disrupts the polypeptide backbone. The YFP labels cytoplasm (A and B, left) while GFP is secreted out of the cells (A, C, and E, right) or appears in the ER network (B, D, and F, right). The RFP is successfully targeted into nucleus (C and D, left) or Golgi apparatus but unexpectedly accumulates in the central vacuole of cells expressing high levels of the STN-$R_m$-2A constructs (E and F, left). secRFP accumulates exclusively in the appoplast (G) while secRFP-2A is almost exclusively vacuolar. Shown are single sections (A and B first row; C and D) and projections (A and B, second and third row; E–H). Scale bar 100 $\mu$m (A and B, first row), 10 $\mu$m (A and B, second row, G and H), and 5 $\mu$m (A and B, third row; C–F).

*et al*., 2000; Kotzer *et al*., 2004; Zheng *et al*., 2005). We have also used such images to quantify the intracellular accumulation of secreted GFP (Zheng *et al*., 2005). However, stochastic variation in transient expression efficiency and variable sampling of three-dimensional (3D) space during imaging limit the ability of this approach to resolve differences in marker accumulation between treatments. Furthermore, the approach cannot be applied to individual cells or protoplasts, nor can it be used to quantify changes in the intracellular distribution of markers. Sampling problems associated with the stochasticity of transient expression are exacerbated when individual cells are analyzed at higher magnification and are compounded in differentiated vacuolated cells the 3D organization of the cytoplasm into a thin-curved cortical layer connected by dynamic transvacuolar strands.

## B. Ratiometric Approaches to Quantify Marker Expression and Accumulation

A potential solution to these problems is to provide a stoichiometric baseline reference for the expression efficiency of the trafficked marker. Ideally this should be measurable under the same conditions as the trafficked marker in either transfected protoplasts, single cells, or whole tissues over a broad range of magnifications. This would correct for the variability in marker expression and imaging efficiency while providing a means to normalize between experiments. The availability of spectrally distinct fluorescent proteins and the instrumentation to distinguish their signals facilitate this approach using ratiometric imaging techniques. When cell populations are analyzed, simply cotransfecting the effector or assay construct with a visible marker on the same or separate plasmids can help to normalize for experiment-to-experiment variation in either protoplast or leaf systems (Lee *et al*., 2002; Samalova *et al*., 2006). Experiments involving the cotransfection of two visible markers show, however, that this can still result in significant cell-to-cell variation in the relative expression level of each marker (Samalova *et al*., 2006). This precludes the use of such strategies to determine the expression level of a cotransfected effector or assay construct in individual cells. Here we discuss in detail the utility of a recently developed approach that uses polyproteins based on the foot and mouth disease virus (FMDV) ''self-cleaving'' 2A peptide (Halpin *et al*., 1999; Ryan *et al*., 1999). These polyproteins express the fluorescent marker and a spectrally distinct fluorescent reference marker from a single open-reading frame, which is translated to generate two separate polypeptides in stoichiometric amounts (Fig. 3). The FMDV-2A-based constructs offer greatly improved sensitivity, objectivity, and statistical robustness in the quantitative assays of biosynthetic membrane traffic in plant cells (Samalova *et al*., 2006). They allow the expression level of a trafficked marker to be inferred from the accumulation of a spectrally distinct fluorescent marker in another cellular compartment so that cells expressing similar and appropriate amounts can be compared. This should help to avoid problems associated with markers becoming missorted or accumulated in upstream compartments simply through overexpression. We describe imaging protocols and analysis tools to quantify marker expression and to facilitate ratiometric

membrane trafficking assays with these FMDV-2A-based constructs in cell populations or individual cells of either stable transgenic plants or transfected cell populations.

### C. FMDV-2A-Based Ratiometric Assays of Marker Expression and Accumulation

The FMDV 2A peptide is a 20 amino-acid peptide that promotes the separation of the 2A and 2B viral translation products from a polyprotein. It disrupts the polypeptide backbone between the terminal glycine and the proline residues of a highly conserved Pro-Gly-Pro motif at the C-terminus of the 2A sequence. The mechanism is apparently protease independent and occurs early relative to the emergence of the polypeptide from the ribosome exit channel (Ryan *et al.*, 1999). Current models suggest that the FMDV 2A peptide (hereafter referred to simply as 2A) acts as an esterase to hydrolyze the link between the nascent polypeptide and the t-RNA in the ribosome P-site before the formation of the terminal Gly-Pro bond of 2A (Ryan *et al.*, 1999). As the translation of the remainder of the ORF can proceed after 2A-mediated hydrolysis, sequences upstream and downstream of 2A are translated as distinct polypeptides from the same ORF in a fixed stoichiometry. The precise stoichiometry can vary between constructs in a sequence-dependent manner, depending on the frequency of ribosome dissociation at the FMDV 2A sequence (Ryan *et al.*, 1999).

As the two translation products emerge independently from the ribosome, it is expected that targeting information in each one may be processed independently by the cell (de Felipe and Ryan, 2004; de Felipe *et al.*, 2003; El Amrani *et al.*, 2004; Samalova *et al.*, 2006). In accordance with this, it has proven that it is possible to generate 2A-based polyprotein fusions in which a GFP molecule is targeted to the secretory pathway or ER while a coexpressed reference marker is targeted to the cytoplasm or nucleus (Fig. 3). It has also been possible to target two proteins to different compartments of the endomembrane system (Fig. 3), though in this case it was observed that the upstream moiety of the polyprotein was sorted efficiently to the vacuole owing to serendipitous vacuolar sorting determinant within the 19 residues of 2A sequence that remain attached to the C-terminus of the amino-terminal cleavage product (Samalova *et al.*, 2006) (Fig. 3G and H). The 2A-cleavage product was observed in the same PVC as the vacuolar-targeted GFP, and its sorting to the vacuole was sensitive to inhibition by a dominant-negative mutant of a Rab-F2 GTPase, suggesting that it followed the conventional route from the Golgi.

### D. Quantitative Imaging of Secreted GFP Accumulation Using FMDV-2A-Based Polyproteins

The pH sensitivity of GFP derivatives in the cell wall has allowed secreted GFP molecules to be used to report on biosynthetic membrane traffic in tobacco and *Arabidopsis* tissues (Batoko *et al.*, 2000; Zheng *et al.*, 2004). Reduced traffic to the cell wall is revealed as increased intracellular accumulation with a concomitant increase in the total fluorescence that accumulates in the tissue. While this provides an obvious qualitative visual assay, its quantification is less straightforward,

as discussed above. We have developed two approaches to using the FMDV-2A-based constructs to quantify secGFP accumulation. The first uses a cytoplasmic YFP as a reference construct and is most suitable for the analysis of cell populations imaged at relatively low magnification when cytoplasm and ER are not well resolved. The second is applicable to individual cells and uses a nuclear-targeted RFP in conjunction with a specific image analysis package. The imaging protocols below are developed to analyze transfected tobacco leaf epidermal cells transiently expressing the fluorescent markers, but they can be adapted to other types of sample such as protoplasts or transgenic plants. The technical specifications relate to the Zeiss LSM 510 confocoal laser scanning microscope.

## III. Material

I. Plant material

*Nicotiana tabacum* SR1 (*cv* Petit Havana) plants grown in potting compost at 20–22 °C constant light for 6–8 weeks.

II. Reagents

A. Bacterial LB medium: 1% (w/v) bacto tryptone, 0.5% (w/v) bacto yeast extract, and 1% (w/v) sodium chloride; pH 7.0; autoclaved.

B. Infiltration medium: 50 mM MES pH 5.6, 0.5% (w/v) glucose, 2 mM $Na_3PO_4$, and 100 $\mu$M acetosyringone (Aldrich) prepared from 1 M stock in DMSO.

C. 5% pleuronic (Molecular Probes)

D. Insulating tape and 3 mm micropore surgical tape

III. CLSM and software

Zeiss LSM 510 laser-scanning microscope or equivalent

Zeiss AIM software version 3.0 or 3.2

Image analysis software available from the authors

## IV. Methods

### A. Method I: Ratiometric Analysis of GFP Secretion in Populations of Cells Using YFP-2A-secG and YFP-2A-GH

1. Background

YFP-2A-secG and YFP-2A-GH express cytoplasmic YFP in stoichiometric quantities with either secreted or ER-resident GFP, respectively (Fig. 3). When $Y_m$-2A-GH was expressed in tobacco leaf epidermal cells, a close correlation was

observed between the YFP and the GFP signals in individual cells over a wide range of intensities (Samalova *et al.*, 2006). Using the protocol outlined below, the GFP and the YFP fluorescence intensities can be measured in low-magnification confocal images and used to express the GFP accumulation either as an absolute value or as a ratio normalized to the YFP value for each image. The high correlation between the GFP and the YFP accumulation was manifested in a marked improvement in the quality of ratiometric over the absolute measurements of GFP accumulation, with the mean coefficient-of-variance being more than twofold lower when the ratio was calculated (Samalova *et al.*, 2006). Furthermore, when $Y_m$-2A-GH was transfected using a 30-fold range of *Agrobacterium* titres, the absolute GFP accumulation varied ~10-fold but the ratio of GFP:YFP varied only 1.4-fold. The ratio was unchanged above $OD_{600}$ 0.05 and was linear up to this point, suggesting that an $OD_{600}$ close to 0.05 is optimal for the use of constructs like $Y_m$-2A-GH. The coefficient of variance for the ratio data was threefold lower than that for the absolute fluorescence data at this $OD_{600}$ or less. Thus the 2A-constructs offer an effective strategy for the ratiometric analysis of GFP expression levels in individual cells and in cell populations, with the YFP accumulation reliably predicting GFP expression efficiency in each cell.

$Y_m$-2A-sec$G_f$, which expresses secreted GFP rather than ER-resident GFP, provides a ratiometric assay for biosynthetic traffic. When this construct is expressed in tobacco leaf epidermis, GFP fluorescence is almost undetectable under imaging conditions that detect the GFP signal from the ER of cells expressing $Y_m$-2A-GH. In cells expressing $Y_m$-2A-sec$G_f$, inhibition of secGFP traffic is expected to increased GFP fluorescence owing to the accumulation of fluorescent GFP in intracellular compartments (Samalova *et al.*, 2006). For example, traffic between the ER and the Golgi can be inhibited by the expression of the dominant-negative N121I mutant of the *Arabidopsis* Rab GTPase *At*Rab-D2[a] (ARA5; AtRab1b; At1g02130). When the absolute and ratiometric measurements were used to quantify the accumulation of GFP in leaf areas, transiently expressing $Y_m$-2A-sec$G_f$ or $Y_m$-2A-GH either alone or with *At*Rab-D2[a] [N121I], both measures revealed an increase in secGFP fluorescence but they differed in two notable ways. First, the ratiometric approach revealed that secreted GFP accumulated to levels comparable to that of the ER-resident GFP-HDEL (expressed from $Y_m$-2A-GH), whereas the absolute expression data in this and previous studies suggested a figure of only 50–75% of GFP-HDEL. This can be explained most simply by a previously undetected reduction in transient expression efficiency in leaf areas coinfiltrated with the *At*Rab-D2[a] [N121I] mutant strain. Second, the Rab mutant also caused a small but significant ($P = 0.05$) increase in the accumulation of GFP-HDEL owing most probably to the escape of some GFP-HDEL molecules from the ER in cells expressing $Y_m$-2A-GH alone. As in other cases, ratiometric analysis increased the statistical significance of the data as illustrated by the lower coefficients of variance between means of different experiments.

## 2. Protocol

### A. *Agrobacterium tumefaciens*-mediated transient expression

1. Using standard cloning techniques, prepare and transform the desired fluorescent constructs into *Agrobacterium tumefaciens.*
2. Grow the *Agrobacterium* in LB medium supplemented with appropriate antibiotics at 28°C for 12–24 h.
3. Spin down 1 ml of the culture, wash the pellet in infiltration medium, firstly without and secondly with acetosyringone, and resuspend to an $OD_{600}$ of 0.05–0.06 for 2A-based markers and empirically determined $OD_{600}$ for effector constructs (the lowest $OD_{600}$ that exerts a statistically significant measurable effect is optimal).
4. Infiltrate the bacterial suspension into the lower (abaxial) leaf epidermis of tobacco leaf using a 1 ml of plastic syringe by applying light pressure with a gloved finger at the opposite side of the leaf. Use sections of leaf separated by primary veins for each sample and mark infiltrated (darkened) areas with a permanent pen.
5. Incubate tobacco plants for further 36–60 h at 20–22°C before examining by CLSM.

### B. Sampling and confocal imaging

1. Prepare a slide by placing two 5–10 mm strips of insulating tape ~40 mm apart and place a drop of 0.5% pleuronic in the center.
2. Excise a piece of leaf from within each marked area and mount with the abaxial side upward into the pleuronic.
3. Place a 50 mm cover slip onto the slide ensuring that the edges do not extend beyond the insulating tape.
4. Cut two 60–70 mm pieces of 3 mm micropore tape approximately and attach to the lower side of the microscope slide beneath the edges of the cover slip. Fold the tape over the top of the cover slip to fix it in place. This ensures that the slide and cover slip will remain flat and level on the stage.
5. Gently tap the cover slip to eliminate trapped air bubbles but avoid any saturation of leaf tissue by the mounting fluid.
6. Adjust the quantity of 0.5% pleuronic under the cover slip so that the leaf pieces are surrounded by a thin film of liquid maximizing the air space between them.
7. Set up the microscope configuration for simultaneous imaging of mGFP5 and YFP as summarized in Fig. 2. Adding a chlorophyll channel can also be useful to aid focusing.

8. Use a 10×/0.3 NA objective lens, 0.7–1× zoom and pinhole aperture to give an optical section of 30 $\mu$m.
9. Set the detector gains to avoid saturation in the brightest samples and amplifier offset to minimize pixels with a value of 0 in the vacuoles of the dimmest samples in the experiment.
10. Collect at least nine images (12-bit) of each sample and also uninfiltrated areas of the leaf to estimate the background fluorescence. Focusing on the chloroplasts helps to ensure that the plane of focus is at a similar point in the tissue to that of the other samples.

C. Extracting data and calculations

1. Record the average GFP and YFP pixel intensity in each image using the histogram function of the Zeiss AIM software version 3.0 or 3.2.
2. Calculate the average background fluorescence for the GFP and YFP channels from the uninfiltrated sample and subtract this value from the GFP and YFP values measured.
3. Calculate the GFP:YFP ratio for each image by dividing the background subtracted values.
4. Calculate the average GFP:YFP ratio and standard deviation for each sample.

## B. Method II: Ratiometric Analysis of Biosynthetic Traffic in Single Cells Using nlsRFP-2A-secG and -GH

### 1. Background

This method utilizes nlsRFP$_m$-2A-secG$_f$ of Samalova *et al.* (2006), which expresses a nuclear-targeted mRFP1 in stoichiometreic quantities with a secreted GFP (Fig. 3). An image analysis tool was developed to quantify the intracellular accumulation of GFP and relate it to the expression level in individual cells imaged at high magnification. The ER-resident GFP signal from the nlsRFP$_m$-2A-GH construct acted as a positive control for the signal intensity that could be expected when anterograde traffic was inhibited (Fig. 3). The example described below is from transfected tobacco leaf epidermal cells, but this method could be applied equally well to transfected protoplasts or cells of transgenic plants. Similarly, the same method could be adopted with YFP-2A-secG and YFP-2A-GH.

Figure 4 presents a flow chart of the procedures that are implemented by the software, depending on the parameters and options chosen by the user in various check boxes on the interface. The step-by-step instructions are given below, but the procedure is presented in outline here. To measure signals unambiguously from specific cells, analysis is performed on the nucleus and perinuclear region of a series

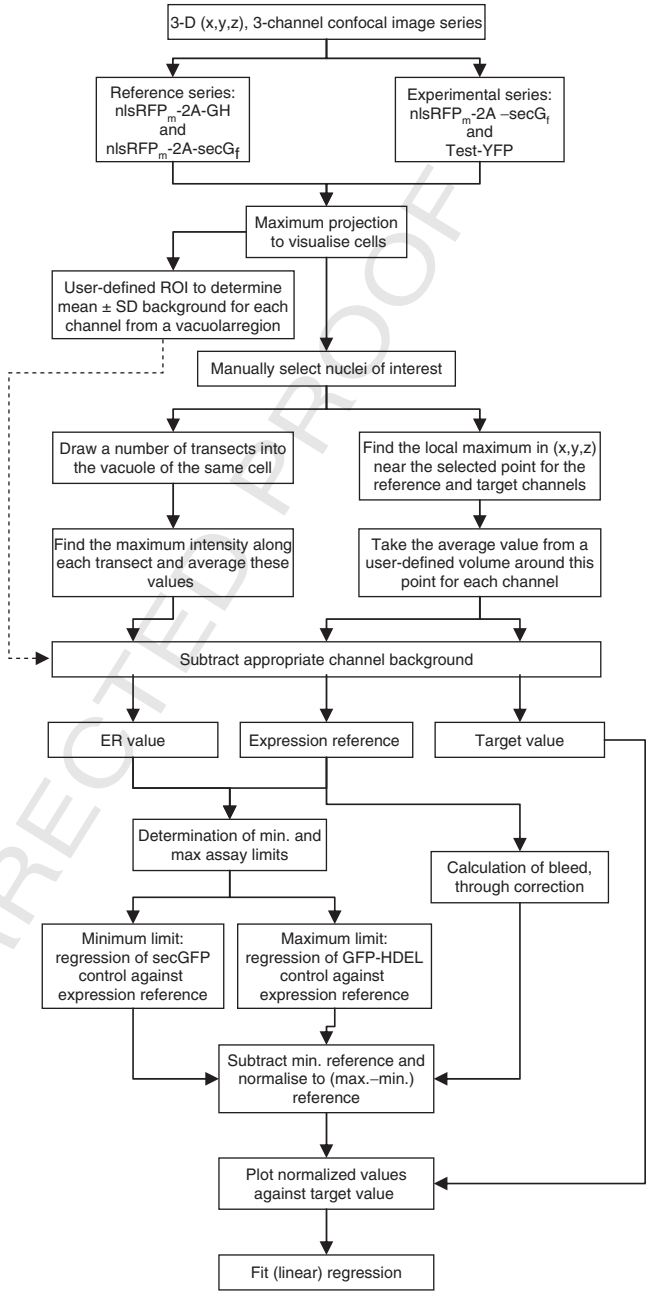


**Fig. 4** Flow diagram of the semiautomated ratiometric image-analysis procedure. Flow diagram of the semiautomated ratiometric image-analysis procedure implemented by the software package illustrated in Figs. 5 and 6.

of confocal sections on the *z*-axis. The software imports the *z*-stacks and presents a maximum projection for the interface with the user (Fig. 5). Starting from a position in the nucleus, the user draws a series of transects across the cytoplasm into the surrounding vacuole of the same cell (see Fig. 5). The nuclear RFP intensity is automatically extracted from the 3D data set from a user-defined seed. The corresponding GFP signal is then sampled along the transects. The GFP values can be plotted against the RFP values to give a slope that can be considered a retention index (RI) for any particular set of imaging conditions. For example, in the data shown in Fig. 6, the RI for nlsRFP$_m$-2A-GH was 2.6 and for nlsR$_m$-2A-secG$_f$ it was 0.022. Thus GFP-HDEL accumulated in the ER 100-fold more efficiently than secGFP in these samples. Note that the dynamic range of this analytical method can be orders of magnitude greater than that of Method I which is typically 5–10 fold (Samalova *et al.*, 2006; Zheng *et al.*, 2005). If the output control of the laser on the confocal system is linear, the dynamic range in this assay can also be extended by increasing the laser intensity used for the excitation of GFP and reducing the intensity used for the excitation of RFP when imaging nlsR$_m$-2A-secG$_f$. This allows more sensitive detection of secGFP without saturation of the nlsRFP values. The GFP and RFP values can simply be divided or multiplied, respectively, by the appropriate factors to render the data equivalent to that obtained for nlsR$_m$-2A-GH. No other imaging parameter should be altered however. The AOTF control on the Zeiss LSM 510 is sufficiently linear for this correction to be made. Our ratiometric image analysis package allows laser intensity correction factors to be entered (Fig. 6).

The effect of a coexpressed protein on secreted GFP accumulation can be most easily determined if this protein can be directly visualized by tagging with YFP. The image analysis tool will automatically extract the YFP value for each cell. The YFP intensity can then be plotted against the GFP-to-RFP ratio for individual cells to generate a slope that gives a measure of the inhibition of biosynthetic traffic. This measure is however an arbitrary statistic that is trivially dependent on the imaging parameters chosen and gives no indication of the biological significance of the inhibition measured. To provide a standard against which to compare the relative data generated by this analysis, the secGFP signal in each cell can usefully be expressed as a percentage of the GFP signal that would be expected for a cell expressing nlsR$_m$-2A-GH at the same level. This can be calculated from the known RFP signal for each cell and a plot of GFP against RFP for nlsR$_m$-2A-GH in the same experiment. These percentages can then be plotted against the YFP values for each cell. The software package will perform this calculation by directly using the appropriate control and the reference data within each experiment. Various metrics can be extracted from such a plot to describe the relative effects of different test constructs. This method can detect secGFP accumulation to just 10% of GFP-HDEL value (Samalova *et al.*, 2006), which would not be measurable using the low-magnification approach owing to the error in the data even with ratiometric analysis. If the YFP-tagged test construct exhibits only a weak effect on

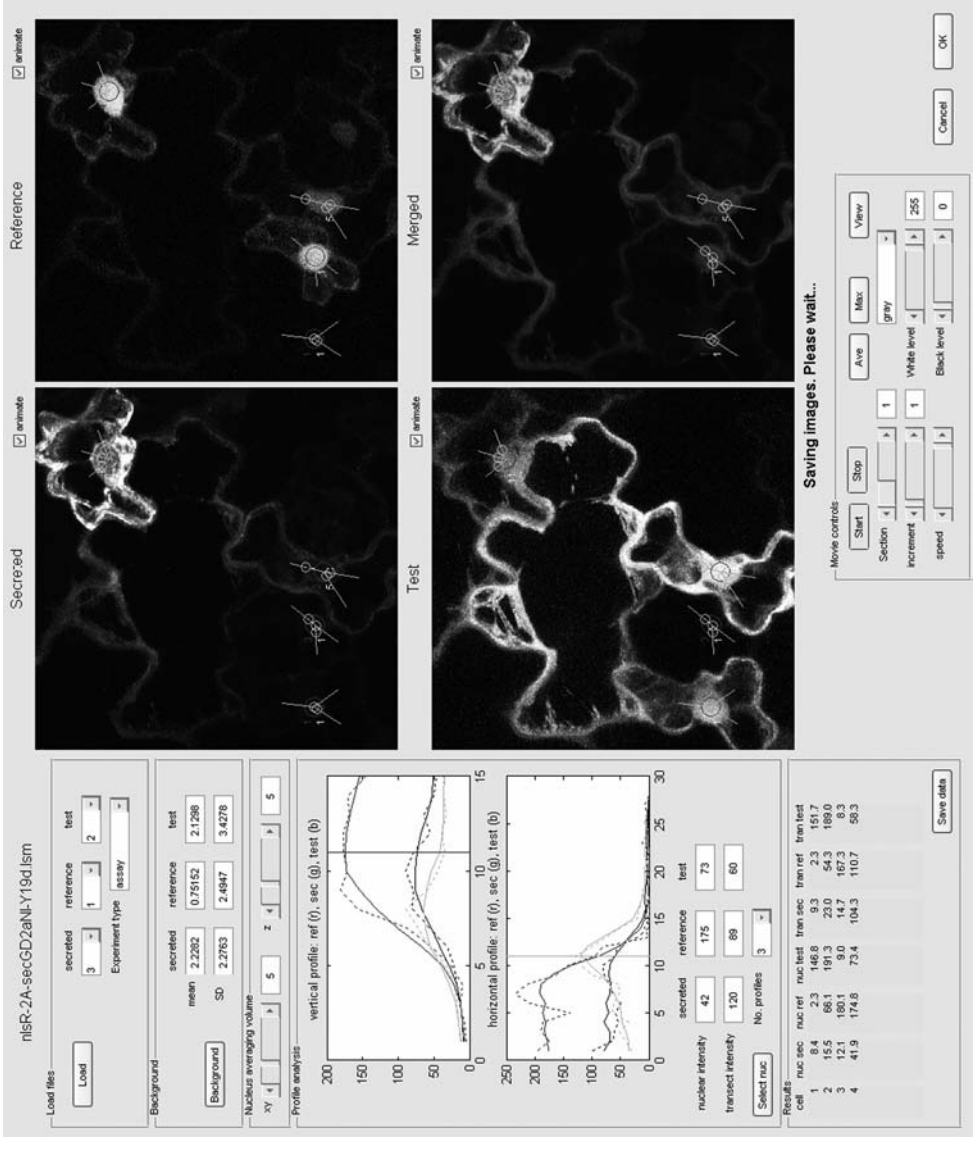


**Fig. 5** Screenshot of the data-extraction interface of the image analysis software. Screenshot (reproduced in black and white) of the data-extraction interface of the image analysis software, illustrated with an image from Fig. 8E–H of Samalova *et al.* (2006) as an example. The three user-defined transects from each selected nucleus are indicated in each image. Secreted refers to the secGFP channel, reference to the nlsRFP channel, and test to the YFP-tagged test or effector construct whose influence on secGFP accumulation is under investigation. Various parameters can be set by the user.

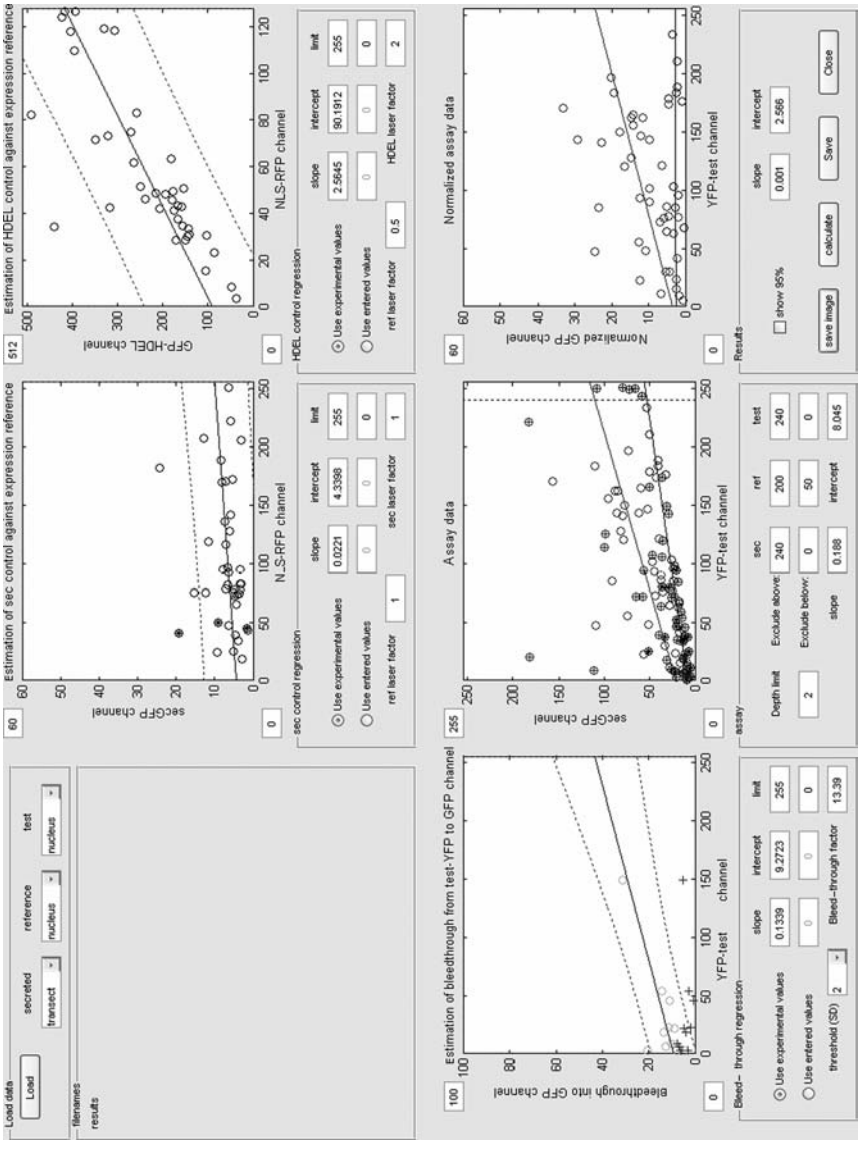


**Fig. 6** Screenshot of the data-analysis interface of the ratiometric analysis software. Screenshot of the data-analysis interface (reproduced in black and white) of the ratiometric analysis software in which the relationships between the GFP, RFP, and YFP values can be determined. The top two graphs show the relationship between the nuclear RFP and the secreted or retained GFP to determined factoring in differences in laser intensities used during image acquisition. Bleed-through from YFP into the GFP channel can also be determined (bottom left). The accumulation of secGFP, normalized for nlsRFP data, is plotted in the lower central graph using the bleed-through correction and user-defined limits on the nlsRFP values (i.e., secGFP expression levels) that are considered worth evaluating. The graph at the lower right expresses the secGFP accumulation data relative to the upper (100%) and lower (0%) limits determined by the analysis of cells that express the ratiometric secGFP or GFP-HDEL markers only.

secGFP accumulation, meaningful data will be obtained only from relatively highly expressing cells. Under these circumstances, it is likely that a bleed-through correction will be necessary to eliminate the YFP contribution to the apparent secGFP accumulation values (Samalova *et al.*, 2006). The software allows this to be calculated and factored into the final analysis (Fig. 6). Bleed-through can be calculated either from a sample infected by the YFP-tagged construct only or by instructing the software to extract data from the cotransfected cell population in which the nlsRFP values are below a user-defined threshold indicating that the cell expresses minimal secGFP.

If the protein under investigation cannot directly be visualized, its effect on secGFP accumulation will be more difficult to measure with this method than with the low-magnification method. At sufficiently high coexpression levels, the average RI for a population of cells will give an indication of the strength of the inhibition, but the data is likely to be noisy unless coexpression approaches 100%. At lower coexpression levels, alternative statistical approaches based on the frequency distribution of GFP:RFP values could be used to identify and quantify a shift in the population as a result of marker expression.

## 2. Protocol

### A. *Agrobacterium tumefaciens*-mediated transient expression

See above (Method I).

### B. Sampling and confocal imaging

1. Prepare the sample for imaging following steps B1–B6 of Method I above.
2. Set up the microscope configuration for simultaneous imaging of mGFP5, mRFP1, and YFP, as summarized in Fig. 2, using whichever of the two triple-track line-sequential imaging configurations gives the best balance of sensitivities for each fluorescent protein at the requisite expression levels.
3. Use 40× objective lens (C-Apochromat 40×/1.2 NA W corr), 1–1.5 zoom, and 1 Airey unit pinhole aperture (ca. 1 $\mu$m optical sections).
4. Set the detector gains to avoid saturation in the brightest samples and amplifier offset to minimize pixels with a value of 0 in the vacuoles of the dimmest samples in the experiment.
5. Collect 3D image stacks (12-bit or 8-bit if the image size is too big) with pixel spacing of $0.3 \times 0.3 \times 2$ $\mu$m or $0.22 \times 0.22 \times 1$ $\mu$m in $x$, $y$, and $z$, respectively, of each sample and also uninfiltrated areas of the leaf to estimate the background fluorescence. The number required will depend on the infection rate and the statistical significance required.

C. Extracting data and calculations

1. Import the 3D image stacks into the Matlab environment (The MathWorks, Natick, MA).
2. Spatially, average the images with a user-defined kernel, typically $3 \times 3 \times 3$ or $3 \times 3 \times 5$, in *x, y*, and *z*, respectively.
3. Visualize data as a maximum brightness projection.
4. Measure the average background signal from each channel using a user-defined region-of-interest chosen to avoid any morphological features, typically from the vacuole in a single plane of the *z*-stack.
5. Manually select nuclei in cells of interest from the maximum brightness projection.
6. Extract the location of the brightest pixel in *z* for the selected (*x* and *y*) pixel. In the nuclear region, this value typically corresponds to the midplane of the nucleus.
7. Measure the average nlsRFP and YFP intensity from the nucleus of selected cells at the selected (*x, y*, and *z*) pixel coordinates. Although the YFP signal is distributed throughout the cytoplasm, the nucleus is chosen to quantify the YFP intensity, as intensity values here are more homogeneous. Nevertheless, the software does offer a choice between nuclear kernel and transect for extraction of intensity values in each channel.
8. Subtract the appropriate average background signal to give the estimated RFP and YFP signals:
9. Draw a number of user-defined transects into the adjacent vacuole from the seed pixel at the selected *z*-plane. Each transect thus spans the nuclear envelope and a thin layer of cytoplasm adjacent to the nucleus. The level of ER-localized GFP is estimated from the average of the brightest features along each transect, following the subtraction of the appropriate background. The corresponding YFP signal is also recorded to calculate the bleed-through component (see later).
10. Filter the data to exclude cells whose nuclei exhibit nuclear nlsRFP fluorescence below an arbitrary threshold, typically 50–90, to ensure sufficient marker expression for quantification of secGFP accumulation, or above a maximum limit, typically between 200 and 240 to avoid saturation. Similarly, cells exhibiting the YFP and GFP values near saturation are not considered in the analysis, as it is not possible to quantify these intensities accurately. These limits can be entered at the user interface.
11. Determine the bleed-through correction factor to compensate for the YFP emission in the GFP detection channel using cells expressing only the YFP-tagged test fusion. The absence of the ratiometric nls$R_m$-2A-sec$G_f$ fusion is determined from cells with nuclear nlsRFP pixel intensity within $2 \times$ SD of background.

12. Subtract the estimated bleed-through component from the YFP signal in the GFP channel using the YFP transect estimate multiplied by the correction factor.
13. Determine the minimum and maximum expected limits for the overall assay from cells transfected with nls$R_m$-2A-secGFP and nls$R_m$-2A-GH, respectively. Note, to bring the signals from nls$R_m$-2A-GH into the same range as the test constructs, it may be necessary to reduce the relative intensity of the 458 nm laser (or the GFP-HDEL signal by up to twofold, and increase the 543 nm excitation intensity for the nlsRFP signal by a similar amount. As fluorescence brightness scales linearly with changes in laser intensity, the corresponding intensity values are rescaled postcapture by introducing the appropriate factors in the interface boxes for the secGFP and GFP-HDEL data.
14. Fit (linear) regressions to the secGFP and rescaled GH data to determine the relationship between the expected minimum and maximum limits for the assay with the overall expression level of the reporter construct, estimated from the nlsRFP signal. As the biological system can saturate with very high ER-accumulation in the HDEL calibration, it may be necessary to only fit a subset of the GH data. The exclusion limits can be set by the user based on the nlsRFP values for each cell.
15. Normalize the corrected GFP signal to the assay limits determined from the regression equations for the corresponding nlsRFP signal and express as a percentage.
16. Plot the normalized secGFP signal against the level of test construct (the YFP signal) and estimate the relationship using (linear) regression.

All the operations described above have been implemented in the stand-alone MatLab software package available from the authors.

## V. Discussion

### A. Quantitative Ratiometric Analaysis of secGFP Accumulation

While nonratiometric approchaes to secGFP accumulation (Zheng *et al*., 2005) are suitable for quantifying large changes in secreted GFP accumulation in transfected tobacco epidermis, the two approaches described by Samalova *et al*. (2006) improve these assays in several ways. First, when used in conjunction with the low-magnification imaging approach described by Zheng *et al*. (2005), ratiometric Method I reduces the error associated with the variable transfection rates and the variable sampling of 3D space within and between experiments. It also normalizes for systematic variations in transfection rates between treatments. These allow the influence of a test construct to be established with greater accuracy and statistical support. Second, Method II allows a more powerful quantitative

analysis of marker accumulation in individual cells. This procedure has a far higher dynamic range, with the secreted and ER-resident GFP markers exhibiting up to a 1000-fold difference in the slope of a plot of accumulation versus expression, in contrast to the approximately fivefold difference they exhibit in absolute fluorescence signals that are measured by the low-magnification assay described by Zheng *et al*. (2005). The low-dynamic range of the low-magnification approach may result from an underestimate of the background fluorescence in the control samples and this may be an aspect of the method that can be improved. Nevertheless, the ability to distinguish between treatments with very similar means is limited principally by the sampling error in the assay, which demands that multiple independent assays are conducted.

In contrast, the single-cell assay allows numerous data points to be extracted from a single transfection, while the low but accurately measured background and high dynamic range allows much improved estimates of small variations in secreted GFP accumulation. It also allows saturation phenomena to be identified and data to be collected only from cells with appropriate expression levels (Samalova *et al*., 2006). Furthermore, it is more versatile than the low-magnification approach being insensitive to transfection efficiency and equally applicable to transfected tobacco epidermal cells, transfected protoplasts, or cells of whole transgenic plants. In the latter case, it has the potential to correct for variations in marker expression or imaging efficiency in various cell types and for epigenetic variation in marker expression within and between individuals or between wild-type and mutant individuals. Indeed, epigenetic cell-to-cell variation within the cells of a transgenic plant or between siblings in a transgenic line could be beneficially utilized to plot accumulation against expression level.

The ratiometric analysis of individual cells requires software which is available on request (mark.fricker@plants.ox.ac.uk) and an imaging system that can discriminate mGFP5 (K. Siemering, S. Hodge, J. Haseloff, MRC Laboratory of Molecular Biology, Cambridge, UK), YFP, and mRFP1. mGFP5 has the advantage over EGFP that it retains the 405 nm excitation peak, allowing it to be more easily discriminated from YFP if a suitable excitation source is available. Alternatively, as YFP can be used in place of GFP in assays of biosynthetic membrane traffic (Geelen *et al*., 2002), nlsRFP$_m$-2A-secYFP or CFP$_m$-2A-secYFP constructs could be assembled and used in conjunction with test proteins tagged with CFP or RFP, respectively. The image analysis software currently measures secreted GFP accumulation in the nuclear envelope and adjacent cytoplasm, as this represents an easily identified and standardized region of the cell. This clearly allows quantification of defects in early stages of biosynthetic traffic, but it may also be applicable to proteins that act at later stages, as it has been shown in two such cases that secGFP accumulates in the ER as well as the Golgi in transfected epidermal cells (Geelen *et al*., 2002; Zheng *et al*., 2005). We envisage that the image analysis tool could be modified to measure accumulation in punctate compartments and to measure other aspects of trafficking, such as vacuolar versus either cytoplasmic or apoplastic accumulation of secN-R$_m$ relative to GFP-HDEL using the secN-R$_m$-2A-GH

construct. Interestingly, the steady-state levels of the secN-$R_m$ moiety of secN-$RFP_m$-2A-sec$G_f$ in the Golgi relative to ER or PVC were substantially lower than those of the sec$G_f$ moiety. It is possible, therefore, that the secN-$R_m$ moiety reaches the PVC and the vacuole without traveling through the Golgi. However, its traffic to the vacuole is inhibited by dominant mutants of the Rab-F2 subclass that also act on the bacuolar trafficking of secGFP and other markers such as aleu-GFP that traffic via the Golgi (Kotzer *et al*., 2004; Samalova *et al*., 2006; Sohn *et al*., 2003). Alternatively, therefore we suspect that secN-$R_m$ is removed from the Golgi more efficiently than sec$G_f$, perhaps as a result of the active vacuolar sorting machinery.

Importantly, nls$R_m$-2A and $Y_m$-2A fusions behave similarly in the two commonly used model organisms, tobacco and *Arabidopsis*. We also envisage that this assay may allow the minimally invasive *Agrobacterium*-mediated transient expression system to be applied in *Arabidopsis* where transfection rates are too low for the low-magnification approaches that have been applied in tobacco. This would obviate the need to use highly perturbed protoplast systems for transfection. Our current attempts suggest that transfection rates are sufficient for ratiometric assays of membrane traffic to be assayed in leaves of mutant or transgenic plants but efficiency will need to be improved if ratiometric markers are to be effectively coexpressed with dominant-interfering proteins.

## B. Future Developments of 2A-Mediated Ratiometry of Membrane Traffic in Single Cells

Simple use of the single cell approach to determine the effect of a coexpressed protein requires either that all cells indeed express saturating levels of the protein of interest or that the protein can be visualized and its expression level determined directly. If the protein cannot be tagged, the low-magnification approach is most easily applied. The principal reason to leave a protein of interest untagged will be that the tag impairs or alters activity as with some Rab GTPases for example (Kotzer *et al*., 2004; Samalova *et al*., 2006). In an attempt to circumvent this problem, Samalova and colleagues (2006) asked whether the 2A peptide could be used to indirectly monitor the expression level of a Rab GTPase that is sensitive to tagging at its amino-terminus. They used 2A to link a nuclear-targeted RFP to the amino-terminus of the Rab GTPase. 2A-mediated cleavage was expected to leave a single proline at the amino-terminus of the protein. When coexpressed with $YFP_m$-2A-sec$G_f$, cells that expressed the highest levels of nuclear RFP also accumulated the highest amounts of secreted GFP relative to YFP. However, the nls$R_m$-2A-Rab fusion exhibited lower levels of activity than the untagged fusion and it was shown that 2A-mediated cleavage was inefficient. This low efficiency of separation was surprising given the efficient separation of YFP and RFP from GFP in $xFP_m$-2A-sec$G_f$ and $xFP_m$-2A-GH. Subsequent mutational analysis indicated that 2A-mediated cleavage at the C-terminus of mRFP1 and especially YFP is indeed inefficient in plant cells and that the efficient separation of $xFP_m$-2A-sec$G_f$ and $xFP_m$-2A-GH was dependent on the signal peptide of the secGFP and GFP-HDEL moieties. These observations are consistent with

the previous reports that 2A activity in plant cells is influenced markedly by the upstream moiety of the fusion protein (Ma and Mitra, 2002). One potential solution to the problem therefore is to place a polypeptide that promotes efficient 2A-mediated cleavage between the fluorescent protein and the downstream 2A peptide.

## VI. Summary

Fluorescent proteins have had a substantial impact on the way in which plant membrane traffic is investigated. The key advantages and disadvantages of various improved fluorescent proteins have become clear and have been exploited to assay function as well as morphology and location of trafficking components. The potential of fluorescent proteins to reveal quantitative information about membrane traffic is only recently being realized. The use of ratiometric trafficking assays facilitated by software packages discussed here will greatly increase the ease and quality of quantitative fluorescence assays of membrane traffic.

## References

Batoko, H., Zheng, H. Q., Hawes, C., and Moore, I. (2000). A Rab1 GTPase is required for transport between the endoplasmic reticulum and Golgi apparatus for normal Golgi movement in plants. *Plant Cell* **12,** 2201–2217.

Boevink, P., Martin, B., Oparka, K., Cruz, S. S., and Hawes, C. (1999). Transport of virally expressed green fluorescent protein through the secretory pathway in tobacco leaves is inhibited by cold shock and brefeldin A. *Planta* **208,** 392–400.

Boevink, P., Oparka, K., Cruz, S. S., Martin, B., Betteridge, A., and Hawes, C. (1998). Stacks on tracks: The plant Golgi apparatus traffics on an actin/ER network. *Plant J.* **15,** 441–447.

Brandizzi, F., Fricker, M., and Hawes, C. (2002). A greener world: The revolution in plant bioimaging. *Nat. Rev. Mol. Cell Biol.* **3,** 520–530.

Brandizzi, F., Irons, S. L., Johansen, J., Kotzer, A., and Neumann, U. (2004). GFP is the way to glow: Bioimaging of the plant endomembrane system. *J. Microsc.* **214,** 138–158.

Campbell, R. E., Tour, O., Palmer, A. E., Steinbach, P. A., Baird, G. S., Zacharias, D. A., and Tsien, R. Y. (2002). A monomeric red fluorescent protein. *Proc. Natl. Acad. Sci. USA* **99,** 7877–7882.

DaSilva, L. L. P., Snapp, E. L., Denecke, J., Lippincott-Schwartz, J., Hawes, C., and Brandizzi, F. (2004). Endoplasmic reticulum export sites and golgi bodies behave as single mobile secretory units in plant cells. *Plant Cell* **16,** 1753–1771.

DaSilva, L. L. P., Taylor, J. P., Hadlington, J. L., Hanton, S. L., Snowden, C. J., Fox, S. J., Foresti, O., Brandizzi, F., and Denecke, J. (2005). Receptor salvage from the prevacuolar compartment is essential for efficient vacuolar protein targeting. *Plant Cell* **17,** 132–148.

De Felipe, P., Hughes, L. E., Ryan, M. D., and Brown, J. D. (2003). Co-translational, intraribosomal cleavage of polypeptides by the foot-and-mouth disease virus 2A peptide. *J. Biol. Chem.* **278,** 11441–11448.

De Felipe, P., and Ryan, M. D. (2004). Targeting of proteins derived from self-processing polyproteins containing multiple signal sequences. *Traffic* **5,** 616–626.

Di Sansebastiano, G. P., Paris, N., Marc-Martin, S., and Neuhaus, J.-M. (1998). Specific accumulation of GFP in a non-acidic vacuolar compartment via a C-terminal propeptide-mediated sorting pathway. *Plant J.* **15,** 449–457.

El Amrani, A., Barakate, A., Askari, B. M., Li, X., Roberts, A. C., Ryan, M. D., and Halpin, C. (2004). Coordinate expression and independent subcellular targeting of multiple proteins from a single transgene. *Plant Physiol.* **135,** 16–24.

Flückiger, R., De Caroli, M., Piro, G., Dalessandro, G., Neuhaus, J.-M., and Di Sansebastiano, G.-P. (2003). Vacuolar system distribution in *Arabidopsis* tissues, visualized using GFP fusion proteins. *J. Exp. Bot.* **54,** 1577–1584.

Frigerio, L., de Virgilio, M., Prada, A., Faoro, F., and Vitale, A. (1998). Sorting of phaseolin to the vacuole is saturable and requires a short C-terminal peptide. *Plant Cell* **101,** 1031–1042.

Geelen, D., Leyman, B., Batoko, H., Di Sansabastiano, G. P., Moore, I., and Blatt, M. R. (2002). The abscisic acid-related SNARE homolog NtSyr1 contributes to secretion and growth: Evidence from competition with its cytosolic domain. *Plant Cell* **14,** 387–406.

Grignon, C., and Sentenac, H. (1991). pH and ionic conditions in the apoplast. *Annu. Rev. Plant Physiol. Plant Mol. Biol.* **42,** 103–128.

Halpin, C., Cooke, S. E., Barakate, A., El Amrani, A., and Ryan, M. D. (1999). Self-processing 2A-polyproteins—a system for co-ordinate expression of multiple proteins in transgenic plants. *Plant J.* **17,** 453–459.

Haseloff, J. <http://www.plantsci.cam.ac.uk/Haseloff/imaging/GFP.htm>

Irons, S., Evans, D., and Brandizzi, F. (2003). The first 238 amino acids of the human lamin B receptor are targeted to the nuclear envelop in plants. *J. Exp. Bot.* **54,** 943–950.

Kamiya, T., Akahori, T., Ashikari, M., and Maeshima, M. (2006). Expression of the vacuolar $Ca^{2+}/H^{+}$ exchanger, OsCAX1a, in rice: Cell and age specificity of expression, and enhancement by $Ca^{2+}$. *Plant Cell Physiol.* **47,** 96–106.

Kotzer, A. M., Brandizzi, F., Neumann, U., Paris, N., Moore, I., and Hawes, C. (2004). AtRabF2b (Ara7) acts on the vacuolar trafficking pathway in tobacco leaf epidermal cells. *J. Cell Sci.* **117,** 6377–6389.

Kunze, I., Hensel, G., Adler, K., Bernard, J., Neubohn, B., Nilsson, C., Stoltenburg, R., Kohlwein, S., and Kunze, G. (1999). The green fluorescent protein targets secretory proteins to the yeast vacuole. *Biochim. Biophys. Acta* **1410,** 287–298.

Lee, G. J., Sohn, E. J., Lee, M. H., and Hwang, I. (2004). The *Arabidopsis* Rab5 homologs Rha1 and Ara7 localize to the prevacuolar compartment. *Plant Cell Physiol.* **45,** 1211–1220.

Lee, M. H., Min, M. K., Lee, Y. J., Jin, J. B., Shin, D. H., Kim, D. H., Lee, K.-H., and Hwang, I. (2002). ADP-Ribosylation Factor 1 of *Arabidopsis* plays a critical role in intracellular trafficking and maintenance of endoplasmic reticulum morphology in *Arabidopsis*. *Plant Physiol.* **129,** 1507–1520.

Ma, C. L., and Mitra, A. (2002). Expressing multiple genes in a single open reading frame with the 2A region of foot-and-mouth disease virus as a linker. *Mol. Breed.* **9,** 191–199.

Matsushima, R., Kondo, M., Nishimura, M., and Hara-Nishimura, I. (2003). A novel ER-derived compartment, the ER body, selectively accumulates a $\beta$-glucosidase with an ER retention signal in. *Arabidopsis. Plant J.* **33,** 493–502.

Nagai, T., Ibata, K., Park, E. S., Kubota, M., Mikoshiba, K., and Miyawaki, A. (2002). A variant of yellow fluorescent protein with fast and efficient maturation for cell-biological applications. *Nat. Biotechnol.* **20,** 87–90.

Runions, J., Brach, T., Kuhner, S., and Hawes, C. (2006). Photoactivation of GFP reveals protein dynamics within the endoplasmic reticulum membrane. *J. Exp. Bot.* **57,** 43–50.

Ryan, M. D., Donnelly, M., Lewis, A., Mehrotra, A. P., Wilkie, J., and Gani, D. (1999). A model for nonstoichiometric, cotranslational protein scission in eukaryotic ribosomes. *Bioorg Chem.* **27,** 55–79.

Saint-Jore, C. M., Evins, J., Batoko, H., Brandizzi, F., Moore, I., and Hawes, C. (2002). Redistribution of membrane proteins between the Golgi apparatus and endoplasmic reticulum in plants is reversible and not dependent on cytoskeletal networks. *Plant J.* **29,** 661–678.

Samalova, M., Fricker, M., and Moore, I. (2006). Ratiometric fluorescence-imaging assays of plant membrane traffic using polyproteins. *Traffic* **7,** 1701–1723.

Scott, A., Wyatt, S. E., Tsou, P.-L., Robertson, D., and Allen, N. S. (1999). A model system for plant cell biology: GFP imaging in living onion epidermal cells. *BioTechniques* **26,** 1127–1132.

Au8

Shaner, N. C., Steinbach, P. A., and Tsien, R. Y. (2005). A guide to choosing fluorescent proteins. *Nat. Methods* **2,** 905–909.

Snapp, E. L., Hegde, R. S., Francolini, M., Lombardo, F., Colombo, S., Pedrazzini, E., Borgese, N., and Lippincott-Schwartz, J. (2003). Formation of stacked ER cisternae by low affinity protein interactions. *J. Cell Biol.* **163,** 257–269.

Sohn, E. J., Kim, E. S., Zhao, M., Kim, S. J., Kim, H., Kim, Y. W., Lee, Y. J., Hillmer, S., Sohn, U., Jiang, L. W., and Hwang, I. W. (2003). Rha1, an *Arabidopsis* Rab5 homolog, plays a critical role in the vacuolar trafficking of soluble cargo proteins. *Plant Cell* **15,** 1057–1070.

Swarup, R., Kargul, J., Marchant, A., Zadik, D., Rahman, A., Mills, R., Yemm, A., May, S., Williams, L., Millner, P., Tsurumi, S., Moore, I., *et al.* (2004). Structure-function analysis of the presumptive *Arabidopsis* auxin permease AUX1. *Plant Cell* **16,** 3069–3083.

Takeuchi, M., Ueda, T., Sato, K., Abe, H., Nagata, T., and Nakano, A. (2000). A dominant negative mutant of Sar1 GTPase inhibits protein transport from the endoplasmic reticulum to the Golgi apparatus in tobacco and *Arabidopsis* cultured cells. *Plant J.* **23,** 517–525.

Tamura, K., Shimada, T., Kondo, M., Nishimura, M., and Hara-Nishimura, I. (2005). KATAMARI1/MURUS3 is a novel Golgi membrane protein that is required for endomembrane organization in *Arabidopsis*. *Plant Cell* **17,** 1764–1776.

Tamura, K., Shimada, T., Ono, E., Tanaka, Y., Nagatani, A., Higashi, S., Watanabe, M., Nishimura, M., and Hara-Nishimura, I. (2003). Why green fluorescence fusion proteins have not been observed in the vacuoles of higher plants. *Plant J.* **35,** 545–555.

Tamura, K., Yamada, K., Shimada, T., and Hara-Nishimura, I. (2004). Endoplasmic reticulum-resident proteins are constitutively transported to vacuoles for degradation. *Plant J.* **39,** 393–402.

Yang, Y. D., Elamawi, R., Bubeck, J., Pepperkok, R., Ritzenthaler, C., and Robinson, D. G. (2005). Dynamics of COPII vesicles and the Golgi apparatus in cultured Nicotiana tabacum BY-2 cells provides evidence for transient association of Golgi stacks with endoplasmic reticulum exit sites. *Plant Cell* **17,** 1513–1531.

Zheng, H. Q., Camacho, L., Wee, E., Henri, B. A., Legend, J., Leaver, C. J., Malho, R., Hussey, P. J., and Moore, I. (2005). A Rab-E GTPase mutant acts downstream of the Rab-D subclass in biosynthetic membrane traffic to the plasma membrane in tobacco leaf epidermis. *Plant Cell* **17,** 2020–2036.

Zheng, H. Q., Kunst, L., Hawes, C., and Moore, I. (2004). A GFP-based assay reveals a role for RHD3 in transport between the endoplasmic reticulum and Golgi apparatus. *Plant J.* **37,** 398–414.

Au4, 5

Au6, 7

# Author Query

**Methods in Cell Biology, 85**
**Chapter 15**

Dear Author,

During the preparation of your manuscript for typesetting some questions have arisen. These are listed below. Please check your typeset proof carefully and mark any corrections in the margin of the proof or compile them as a separate list. This form should then be returned with your marked proof/list of corrections to Elsevier Science.

**Disk use**

In some instances we may be unable to process the electronic file of your article and/or artwork. In that case we have, for efficiency reasons, proceeded by using the hard copy of your manuscript. If this is the case the reasons are indicated below:

☐ Disk damaged ☐ Incompatible file format ☐ LaTeX file for non-LaTeX journal

☐ Virus infected ☐ Discrepancies between electronic file and (peer-reviewed, therefore definitive) hard copy.

☐ Other: .....

We have proceeded as follows:

☐ Manuscript scanned ☐ Manuscript keyed in ☐ Artwork scanned

☐ Files only partly used (parts processed differently:.....)

**Bibliography**

If discrepancies were noted between the literature list and the text references, the following may apply:

☐ The references listed below were noted in the text but appear to be missing from your literature list. Please complete the list or remove the references from the text.

☐ Uncited references: This section comprises references which occur in the reference list but not in the body of the text. Please position each reference in the text or, alternatively, delete it. Any reference not dealt with will be retained in this section.

| Query Refs. | Details Required | Author's response |
|---|---|---|
| AU1 | Please define the term PM here. | |
| AU2 | Please check the change. | |
| AU3 | Please check the change. | |
| AU4 | Please check the insertion. | |
| AU5 | As per style *et al.* is used in the reference list after 12 author names and rest of the names are deleted. Kindly check for accuracy in all such cases. | |
| AU6 | Please check the change in Yang, Y. D. *et al.* from 1995 to 2005. | |
| AU7 | Please check the insertion of the Article title in Yang Y. D. *et al.* | |
| AU8 | Reference not cited in text. Please check. | |